Formation of Highly Oriented Biodegradable Polybutylene Succinate Adipate Nanocomposites: Effects of Cation Structures on Morphology, Free Volume, and Properties

Katherine M. Dean,[1] Steven J. Pas,[1,2] Long Yu,[1] Anne Ammala,[1] Anita J. Hill,[1,2] Dong Yang Wu[1]

[1]*Commonwealth Scientific and Industrial Research Organization (CSIRO), Division of Materials Science and Engineering, Clayton 3168, Australia*
[2]*ARC Australian center for Electromaterials Science, School of Chemistry and Department of Engineering, Monash University, Clayton VIC 3800, Australia*

Received 18 July 2008; accepted 11 January 2009
DOI 10.1002/app.30041
Published online 14 May 2009 in Wiley InterScience (www.interscience.wiley.com).

ABSTRACT: Many biodegradable polymer materials have not been found to be suitable replacements for more traditional non-biodegradable polymers owing to their insufficient gas and vapor barrier properties. The use of a series of novel organically modified synthetic fluorohectorites (FHTs) has been explored to produce biodegradable polybutylene succinate adipate (PBSA)-clay nanocomposites with improved barrier. Highly oriented nanoclay structures (clearly showing a tortuous path required to reduce gas and vapor transmission) were observed using transmission electron microscopy (TEM), resulting in a significant reduction in oxygen permeability (up to a 53% decrease). In particular, these oriented structures were observed in the FHTs modified with di poly(oxyethylene) alkyl methyl ammonium and the longer chain dimethyl dialkyl ammonium. Orientation and dispersion were found to be a result of chemical functionality, chain length, and unique aspect ratios of these FHTs. It was concluded that this reduction in permeability was predominantly due to the tortuous path created by oriented platelets and not from any nucleating effects the platelets may have had. Interestingly, the FHTs were shown to disrupt crystallinity and no change in free volume (as measured using positron annihilation life-time spectroscopy) was observed. The excellent clay dispersion and orientation also led to significant increases in other properties. © 2009 Wiley Periodicals, Inc. J Appl Polym Sci 113: 3716–3724, 2009

Key words: biodegradable; biopolymers; gas permeation; nanocomposites

INTRODUCTION

There has been significant interest in the development of biodegradable polymers from renewable resources over the past decade, predominantly because of the concerns for the environment and the finite nature of our oil reserves. In conventional petrochemical polymers the formation of nanocomposites has been shown to significantly improve a range of properties. Nanocomposite technology has also been utilized to improve the properties (thermal, mechanical, and barrier) of biodegradable polymers to make them competitive with their petrochemical counterparts. Biodegradable polymers which have been improved by the incorporation of nanoparticles include starches,[1,2] proteins,[3,4] and polyesters (polycaprolactone,[5,6] polylactic acid,[7–10] and other aliphatic polyesters[11–18]). Biodegradable polyesters are a class of biopolymers which currently offer some of the most comparable (thermal, mechanical, and barrier) properties to conventional petrochemical polymers.

Ray et al.[13,14] investigated the effects of adding the hydroxy modified montmorillonite (MMT) clay, Cloisite 30B, and two other modified MMT clays to polybutylene succinic-*co*-adipate (PBSA). Compared with other alkyl modified montmorillonites the 30B showed the most superior dispersion and corresponding improvements in properties (mechanical (59% increase in tensile modulus using 30B) and thermal) owing to the strong interaction of the hydroxy groups in the gallery of the clay and the carboxyl groups of the aliphatic polyester. Interestingly, Ray et al.[13,14] did not find much variation in the yield strength perhaps owing to a drop in crystallinity of the neat PBSA after nanocomposite formation.

Someya et al.[15] and Shih et al.[16] also investigated the effects of the addition of modified MMT in PBSA. Someya et al.[15] used a number of different amine-based modifications (*N*-lauryldiethanolamine

Correspondence to: K. M. Dean (katherine.dean@csiro.au).
Contract grant sponsor: CSIRO Materials Science and Engineering.

(LEA), 12-aminolauric acid (ALA), and dodecylamine (DA) to investigate the effects on hydrophobicity and polar steric interactions. LEA-modified MMT nanocomposites showed the largest intergallery spacing (1.4–1.5 nm). DA, ALA, and LEA all showed good dispersion, according to TEM images. Although tensile modulus was shown to increase, particularly with the LEA modification, tensile strength and elongation were either unchanged or slightly lower than the control PBSA. Shih et al.[16] used a cetyl pyridinium (CP)- and cetyl trimethyl ammonium (CTA)-modified MMT in PBSA. Higher values for the real (storage) modulus were recorded for the nanocomposites, using dynamical mechanical analysis (DMA), in particular for the CTA-modified system. DMA also showed the nanocomposites based on CP had a higher T_g than those based on CTA. The authors suggested that the increase in T_g was possibly because of the aromatic group of CP providing more constraint on the polymer molecular motion than the CTA chain.

To a lesser extent, researchers have also investigated the use of synthetic fluorohectorites (FHTs). FHTs are part of the same 1 : 2 phyllosilicate family of clays as montmorillonites; however, they do exhibit some significant crystallographic differences. Montmorillonites have a permanent layer charge because of the isomorphous substitution, generally in the octahedral sheet (typically from the substitution of low charge species such as Mn^{2+} for Al^{3+}), whereas the FHT has a charge owing to the isomorphous substitution of Li^{+} for Mg^{2+}. The hydroxy (OH) groups that are found in the octahedral sheets of montmorillonites are substituted by fluorine (F) in FHTs, hence the name. Ray et al.[17,18] have investigated the addition of a modified FHT (modified with di poly(oxyethylene) alkyl methyl ammonium) to PBSA through batch mixing, this system produced an intercalated and exfoliated structure, which had a 120% increase in elastic storage modulus (as measured via dynamical mechanical analysis).

Although work has been undertaken on the effects of nanocomposite formation on permeability in other biopolymer systems, such as poly(lactic acid)[10,19] and poly(caprolactone)[20], with success using a number of Na–MMT based systems (around 50% reduction observed in oxygen permeability in PLA using the dimethyl, hydrogenated tallow, two ethylhexyl quaternary ammonium modified montmorillonite at loadings of 5–10 wt %)[10,19] to the authors knowledge no work has been undertaken on the effects of nanocomposite formation on gas and vapor permeability in PBSA systems. Controlling gas and water vapor permeability is critical in many packaging applications and poor barrier is one of the current impediments to market implementation of many biopolymer systems. In barrier type applications, the high aspect ratio of dispersed nanoclays can force gas and water molecules to follow a more tortuous path through the polymer matrix, resulting in larger diffusion distances thereby lowering permeability.[10]

Positron Annihilation Lifetime Spectroscopy, provides a measure of the size and concentration of free volume elements in polymers such as intra- and interchain spacings and free space at chain ends, The PALS experiment uses *ortho*-positronium (*o*-Ps) to determine the size and number of pores. The lifetime of *o*-Ps in a vacuum is 142 ns, but in polymers, this lifetime is shortened to a few nanoseconds. Before annihilation, the *o*-Ps will localize in pores. The *o*-Ps lifetime depends on the probability of the overlap of the *o*-Ps wave function with the wave function of an electron of a molecule making up the pore wall. As the pore gets larger, the probability of wave function overlap decreases so that the *o*-Ps lifetime increases. Hence, the *o*-Ps lifetime reflects the size of the pore. The number of positrons annihilating as *o*-Ps, as determined by the intensity parameter, gives information on the number of pores.

The effect of incorporating modified montmorillonite clays in a polyamide has been studied by PALS[21] with trends in the *o*-Ps lifetimes and intensities suggesting that the free volume of the polymer is not influenced by the clay at concentrations < 19 wt %. Wang et al.[22] have shown that for an epoxy resin/recotrite nanocomposite, the *o*-Ps intensity decreases with increasing clay content, following volume additivity, with the *o*-Ps lifetime remaining constant. Wang et al.[23] have also shown for an epoxy-resin/montmorillonite nanocomposite the *o*-Ps lifetime decreases with increasing clay content, up to 2 wt %, whereas above 2 wt % clay the *o*-Ps lifetime for the nanocomposite is identical to the neat polymer and does not change with further increase in clay content. *o*-Ps intensity was shown to decrease monotonically, following volume additivity, with increased montmorillonite. For both montmorillonite and rectorite epoxy nonocomposites, the decrease in *o*-Ps intensity is attributed to volume filling of the polymer by the clay, as the exfoliated clay platelets do not contain any oPs accessible pores.

The focus of this study is the formation of FHT nanocomposites based on PBSA (aliphatic biopolyesters made via a polycondensation reaction of 1,4 butandiol and succinic acid or adipic acid[24]). This work shows the structure–property relationships of a number of different cation exchanged FHT-based PBSA nanocomposites with a focus on clay dispersion, orientation, and exfoliation, polymer crystallinity, nanocomposite free volume, and gas barrier. Knowledge contributing to the production of biodegradable polymers with adequate mechanical and barrier properties should speed the market implementation of polymers from renewable resources.

EXPERIMENTAL

Materials

The aliphatic polyester used in this study was a polybutylene succinate adipate (PBSA, Bionolle™ 3001, supplied by Showa, Japan, see Fig. 1). Four different synthetic FHT clays (Na–FHT supplied by Unicoop Japan, see Fig. 2) were used in this study of nanocomposite formation, structure, and properties. The organic components of each clay modification were measured using thermal gravimetric analysis and are listed in Table I. The PBSA and nanoclays were dried in a dessicated oven for 24 h at 70°C before processing to remove water, dried materials were added immediately to the extruder.

Experimental

PBSA was extruded with the modified flurohectorites using a Theysohn twin screw extruder (L/D 40) operating at 120 rpm (allowing greater residence time) using an average barrel temperature of 130°C and a final cooling section of 120°C. The screw design included a number of specifically designed high shear sections to encourage exfoliation of platelets. For each unmodified FHT and three modified FHT loadings of 1,2, and 5 wt % were investigated. Extruded pellets were subsequently dried at 70°C for 12 h and then either injection molded at 130°C into standard test pieces for tensile (3 mm thick dogbone sections) and impact testing (3 mm sections) or compression molded at 130°C to produce film (270–300 mm) for permeability, thermal, and PALS analysis.

XRD was predominantly used to monitor the d_{001} spacing corresponding to the intergallery spacing of the Na–FHT. The XRD measurements were performed on the nanocomposite samples using a Bruker D8 Diffractometer operating at 40 kV, 40mA, Cu Kα radiation monochromatized with a graphite sample monochromator. A diffractogram was recorded between 2θ angles of 1° and 10°.

The nanocomposites were imaged using a Phillips CM30 TEM using an accelerating voltage of 100 keV at magnifications of up to 100,000 to study dispersions of Na–FHT particles. The injection-molded samples were sectioned using a 45° diamond knife at -100°C. The 70-nm thick ribbons were carefully sandwiched between two copper grids for imaging using TEM.

The thermal degradation profile of the nanocomposite samples were measured using a Perkin-Elmer

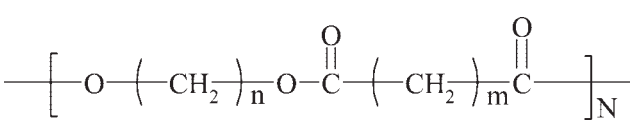

Figure 1 Structure of PBSA.

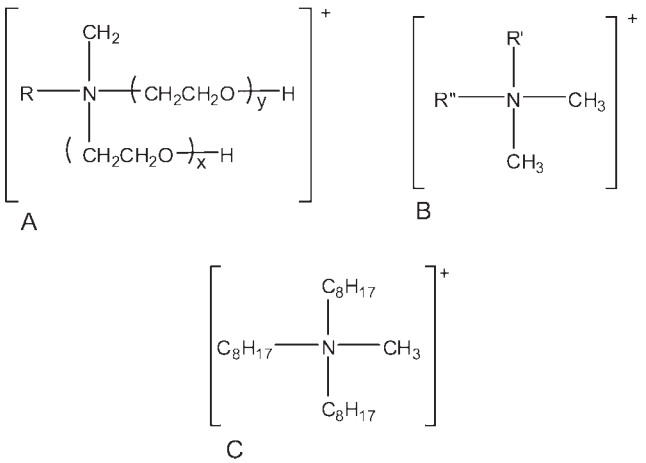

Figure 2 Structures of A: di poly(oxyethylene) alkyl methyl ammonium (where $x + y = 2$ and R is an alkyl chain length not specified by the supplier); B: dimethyl dialkyl ammonium (where R' and R'' are hexadecyl and octadecyl, respectively), and C: Trioctyl methyl ammonium.

Pyris TGA in scanning mode. Approximately 5 mg of the neat polyester and resulting nanocomposites were placed in the pan and scanned from 50 to 800°C at 10°/min.

Differential scanning calorimetry (DSC) was carried out on a Perkin-Elmer Pyris I DSC with intracooler attachment. The temperature and enthalpy were calibrated using high purity indium and zinc standards. Approximately 5–8 mg of the neat polyester and resulting nanocomposites were sealed in aluminum pans and scanned from 25 to 225°C at 5°C / min. Deconvolution of the overlapping melting peaks in all systems was undertaken using percentage area calculations from the Perkin-Elmer Pyris software.

Mechanical testing was undertaken as outlined in ASTM 638 on an Instron tensile testing apparatus (5565) utilizing a 30 kN load cell and a 50 mm/min strain rate. An external extensometer was used for independent modulus measurements. The individual values provided are an average of seven repeats. Impact properties were tested according to ASTM 256 on a Radmana ITR 2000 instrumented impact tester in Izod mode with impact strain rate 3.5 ± 0.2 m/s. The individual values provided are the average of 10 repeats.

Oxygen transmission rate at 23°C, 1 atm, and 0% relative humidity was measured with a MOCON OXTRAN 2/20. The instrument was calibrated with a Mylar film of known oxygen permeability. Films were conditioned for 2 h in the MOCON cells before measurements being taken over a 24-h period. A minimum of three samples were tested for each formulation.

PALS experiments were performed using an EG&G Ortec fast–fast coincidence system with fast plastic scintillators and a resolution function of 260 ps FWHM (^{60}Co source with the energy

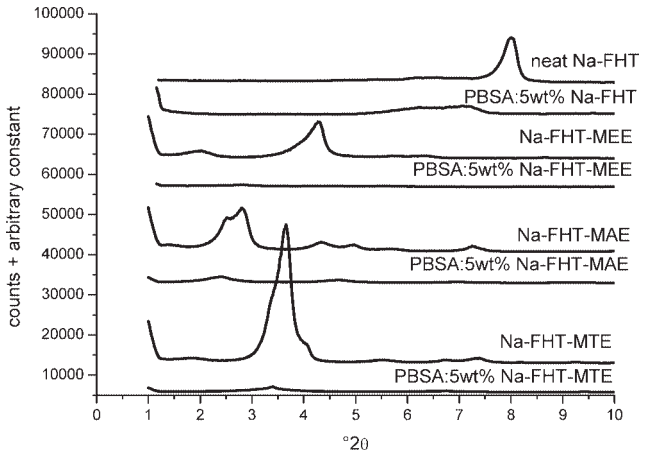

Figure 3 X-ray diffractograms of various Na-FHT clays and their respective nanocomposites with PBSA.

windows set to ^{22}Na events). A stack of ~5 films of each sample was packed on either side of a 30 μCi ^{22}NaCl foil (2.54 μm Ti) source. At least 21 spectra of 500,000 integrated counts were collected with each spectrum taking about 0.25 h to collect. Data analysis was performed using LT9.[25] The spectra were best fitted with three components with the shortest lifetime fixed to 125 ps, characteristic of *para*-positronium (*p*-Ps) annihilation. No evidence of source irradiation damage was observed and no source correction was used. Mean pore radii were calculated from mean lifetimes using the Tao–Eldrup equation.[26,27]

RESULTS AND DISCUSSION

XRD

The neat Na–FHT (as received from the supplier) had a d_{001} spacing of 1.0 nm (8.80°2θ) and another peak at 1.24 nm (7.12°2θ). This peak at 1.24 nm may be associated with bound water, as when the clay was dried under vacuum at 100°C for 12 h this peak disappeared – see Figure 3. According to the supplier of the Na–FHT series, these swellable clays contain H_2O in the crystal interlayer. It is known that interlayer distance expands to 1.26 nm (7.01°2θ) when a monolayer of H_2O is present in the crystal interlayer, to 1.52 nm (5.81°2θ) for a bilayer and to 1.80 nm (4.98°2θ) when three layers of H_2O are present. The number of layers present depends on the relative humidity. Generally, for the samples under consideration, only one layer of water was shown to be present as a peak at 1.26 nm (7.01°2θ) was observed when the relative humidity was below 50%,

When dispersed in the PBSA at loadings of 5 wt %, a range of different states of intercalation and exfoliation were observed in the XRD traces for the nanocomposites formed – see Figure 3. The Na–FHT showed a single peak at 1.0 nm and its corresponding nanocomposite a low-intensity broad double peak with peaks at 1.25 nm (7.07°2θ) to 1.42 nm (6.22°2θ). The neat Na–FHT–MEE containing the hydroxy functionalized clay modification had a main peak at 2.06 nm(4.29°2θ) (smaller peak observed at 4.48 nm (1.97°2θ)) and its corresponding nanocomposite appeared to show the highest level of exfoliation, with the d_{001} peak at 3.15 nm (2.80°2θ) having very low intensity as compared with the Na–FHT–MEE itself, most likely due to the good compatibility between the hydroxy functionalized clay modification and the carboxyl functionalities within the PBSA backbone. The neat Na–FHT–MAE showed more complex behavior having a major peak at 3.69 nm (2.39°2θ) and a range of other smaller peaks giving some indication of the range of different states the clay may have been in (possibly owing to variation in synthesis from the supplier). Even though the clay had a higher initial intergallery spacing, the d_{001} peak was still observed at 3.71 nm (2.38°2θ) after dispersion (although greatly diminished in intensity). Finally, the neat Na–FHT–MTE clay showed a clear d_{001} peak at 2.42 nm (3.65°2θ) and once dispersed into the PBSA (although greatly diminished) was still present at 2.61 nm (3.38°2θ).

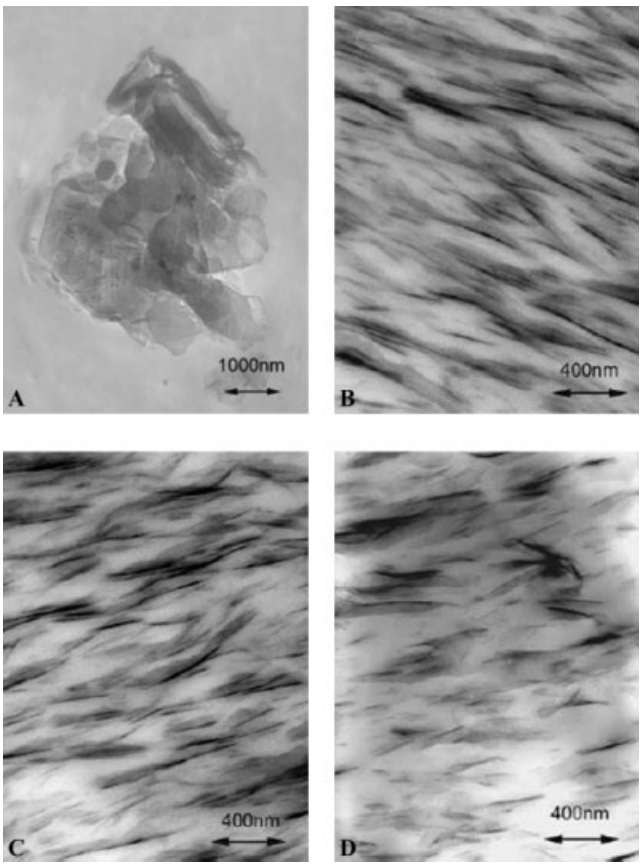

Figure 4 TEM of A: PBSA with 5 wt % Na–FHT; B: PBSA with 5 wt % Na–FHT–MEE; C: PBSA with 5 wt % Na–FHT MAE; D: PBSA with 5 wt % Na–FHT MTE.

TABLE I
Specific Clay Modifications

	Modification	% Organic
Na–FHT	None	0
Na–FHT MEE	Di poly(oxyethylene) alkyl methyl ammonium	25.01
Na–FHT MAE	Dimethyl dialkyl ammonium	37.50
Na–FHT MTE	Trioctyl methyl ammonium	29.00

TEM

The results from XRD were confirmed via TEM imaging (Fig. 4) in which samples containing modified clays showed quite good dispersion of FHT platelets (many single platelets and small tactoids). The highly dispersed and oriented Na–FHT–MEE and Na–FHT–MAE nanocomposites (as seen via TEM) had higher d_{001} spacings (3.15 nm and 3.71 nm, respectively) whereas the d_{001} spacing for the not so well dispersed Na–FHT–MTE remained relatively unchanged from the neat Na–FHT–MTE (2.61 nm as compared with 2.42 nm, respectively). Both chemical functionality (presence of hydroxy groups in the Na–FHT–MEE) and high initial d_{001} spacing (presence of longer alkyl chain hexadecyl and octodecyl groups in Na–FHT–MAE) were advantageous in terms of clay dispersion. In comparison with previous work on MEE by Ray and Bousmina[17] (batch mixing process), the modified FHTs in our research (in particular MEE and MAE) are highly oriented presumably owing to the high shear extrusion processing and injection molding direction employed. The platelets were also very well dispersed and showed clearly the tortuous path required for reducing gas permeability.

TGA

TGA results, as presented in Table II, show that the Na–FHT–MEE (which contains the oxyethylene group) nanocomposite has the least amount of weight loss through the main degradation regions at 400°C and 425°C. The Na–FHT–MEE nanocomposite has retained 15 and 20% more of its weight, respectively, when compared with the neat PBSA and the unmodified Na–FHT-based nanocomposite. Similar low levels of weight loss were also observed for the Na–FHT–MTE nanocomposite system, with 28–30 wt % organic component in the Na–FHT itself.

The nanocomposite containing the dimethyl dialkyl ammonium (MAE) modified FHT with its longer alkyl chains (octodecyl) had a higher organic content than the other two modified clays and thus exhibited greater weight loss throughout the decomposition range starting from around 300°C and continuing onto 500°C. Figure 5 shows a linear relationship between the organic content of each of the Na–FHTs and the weight remaining in the final nanocomposites containing 5 wt % for each of the modified clays.

DSC

DSC of the neat PBSA showed a T_g of -45.9°C (similar to the -45°C reported previously[24]) and subsequent small increases in T_g (up to -43.1°C for the Na–FHT–MTE) for the various FHT nanocomposites (see Table III). The Na–FHT–MEE showed the smallest increase in T_g (a shift of 1.4°C up to −44.5°C) as compared with the neat PBSA, perhaps due to a small plasticizing effect of the di poly(oxyethylene) alkyl methyl ammonium ion as compared with the other alkyl modified FHTs. The neat PBSA showed double melting peaks (at 85.7°C and 94.5°C) owing to two types of crystalline lamellae present as reported by previous authors.[13] The total melting enthalpy of these two overlapping peaks was measured to be 41.5 J/g (close to 43.0 J/g as reported previously by John et al.[28] (see Table III).

Silicate-type additives (such as talc) are well-known nucleating agents for crystallization in polymers,[28] in fact a number of authors have reported similar enhanced crystallization rates and levels[29] using well dispersed Na–MMT layered clays.[29] Previous authors have also found that depending on the nature of the crystalline polymer and dispersion of nanoclays the clays can reduce the level of crystallinity and rate of crystallization by acting as impurities/obstacles to the crystal growth.[14] In all nanocomposite systems shown in this article (unmodified Na–FHT and three modified systems) two melting peaks were

TABLE II
Thermal Behavior of Neat PBSA and Nanocomposites from TGA

Sample	Percentage of original weight at 100°C	Percentage of original weight at 400°C	Percentage of original weight at 450°C
Neat PBSA	99.95	67.85	16.00
PBSA/Na–FHT	99.8	63.67	17.24
PBSA/Na–FHT MEE (25.01% MEE)	99.95	81.23	38.15
PBSA/Na–FHT MAE (37.50% MAE)	99.95	73.70	23.10
PBSA/Na–FHT MTE (29.00% MTE)	99.95	80.40	33.13

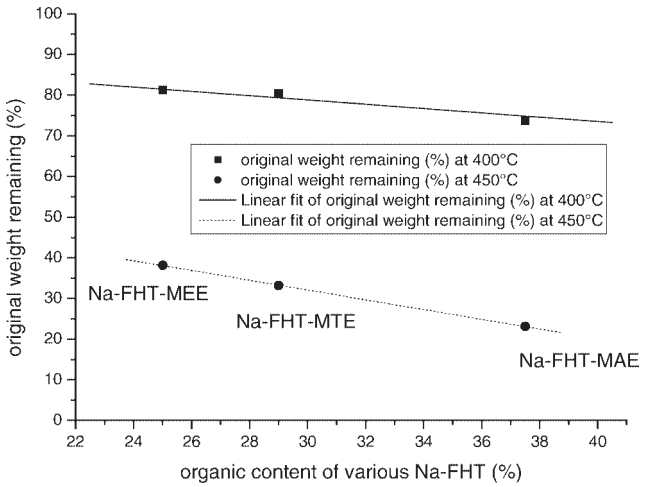

Figure 5 Original weight remaining in nanocomposites (containing 5 wt % modified Na–FHT) versus initial organic content of each of the Na–FHTs.

also observed, showing an overall small decrease in melting enthalpies as compared with the neat PBSA. Interestingly, on further analysis of these melting peaks it was shown that the dominant reduction in enthalpy occurred in the first peak (80–85°C). The peak temperatures for this first melting peak were also reduced in the Na–FHT systems possibly because of the lower value of enthalpy of crystallization of the nanocomposite. In summary, of the two crystalline regions present in PBSA it was the lower melting temperature region which was more affected by the addition of Na–FHT.

Mechanical properties

The tensile strength, modulus and elongation at yield for the addition of 1, 2.5, and 5 wt % of either unmodified Na–FHT, Na–FHT–MEE, Na–FHT–MAE, or Na–FHT–MTE are shown in Figures 6–8.

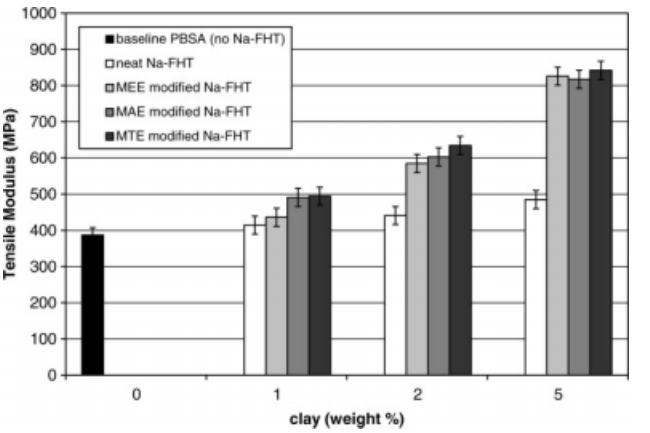

Figure 7 Tensile modulus (MPa) for nanocomposites with variation in clay type and concentration.

The tensile strength increases with increasing clay content and is marginally higher for the Na–FHT–MAE (dimethyl dialkyl ammonium- with C12 and C16 alkyl chains), which also shows well-dispersed platelets in the TEM. The Na–FHT–MEE (di poly(-oxyethylene) alkyl methyl ammonium) shows a slightly lower than expected tensile strength, one would expect that the hydroxyl functionality would have improved the interface between the clay and PBSA. Previous authors have shown that modified montmorillonites (also having hydroxy-based modifications) have not had a significant effect on increasing tensile strength as compared with the neat PBSA.[13] In our system, the tensile strength of Na–FHT–MEE was slightly lower than the unmodified Na–FHT nanocomposites but still higher than the neat PBSA. Although the hydroxy functionality may have improved the interface between FHT and PBSA, the addition of all FHTs (whether modified or not) led to a drop in overall degree of crystallinity which could have had an adverse effect on tensile strength.

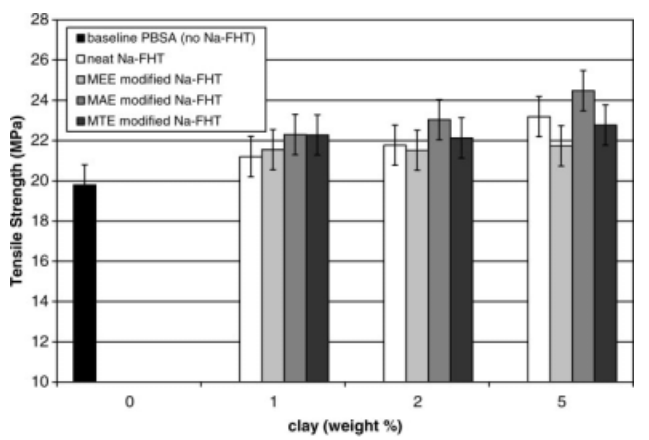

Figure 6 Tensile strength for nanocomposites with variation in clay type and concentration.

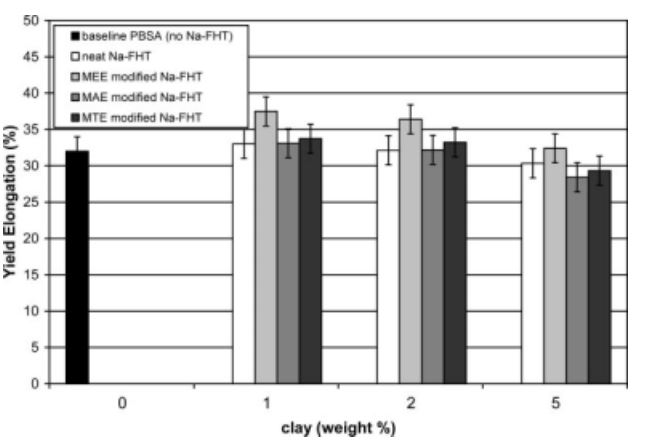

Figure 8 Yield elongation (%) for nanocomposites with variation in clay type and concentration.

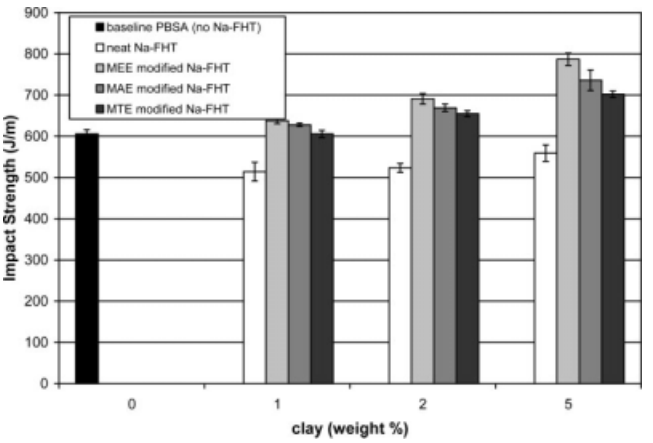

Figure 9 Impact strength (J/m) for nanocomposites with variation in clay type and concentration.

All the three organically modified FHT nanocomposites showed significant increases in modulus (around 120% increase for all three systems at 5 wt % clay loading). This improvement in Young's modulus is attributed to the high modulus of the individual clay layers, the excellent dispersion and orientation of the clays, and the shape and aspect ratios of these clays.[30] The yield elongation increased on the addition of low levels of Na–FHT–MEE. Ray et al.[14] also observed similar effects in Na–MMT systems and suggested that the strong interaction between hydroxy groups from the Na–MMT and the PBSA backbone led to greater confinement of polymer chains between the silicate layers leading to a more efficient energy dissipation mechanism, as more energy would be required to pull the polymer chains apart. This may have also been due to the reduction in crystallinity of the PBSA matrix. For the other systems studied here, yield elongation was similar to the neat PBSA.

The results of impact strength for the addition of 1, 2.5 and 5 wt % of either unmodified Na–FHT, Na–FHT–MEE, Na–FHT–MAE, and Na–FHT–MTE are shown in Figure 9. The Na–FHT–MEE system exhibited the highest impact strength (30% higher than the neat PBSA for the system containing 5 wt % modified clay) owing presumably to the improved interface between NA–FHT–MEE and PBSA. Although it must be noted that the Na–FHT–MAE and Na–FHT–MTE exhibited a 21% and 16% improvement in impact strength as well. Without detailed examination of the fracture surface, further comment on the mechanism of crack initiation and propagation cannot be made.

Free volume measurements

Figure 10 shows the *o*-Ps lifetimes measured from the polymer host, the unmodified clay nanocomposite and the modified clay nanocomposites. As can be seen, there is clearly no difference in *o*-Ps lifetime measured from each of the samples. This result suggests that the nanoparticles (modified or not) have had no effect on the mean size of free volume elements in the polymer matrix. This result is in agreement with previous work at similar loading levels (5 wt %)[21-23]. The *o*-Ps lifetime of 2.15 ns equates to a pore size of 6 Å, which is well above the kinetic diameter of O_2 (3.46 Å).

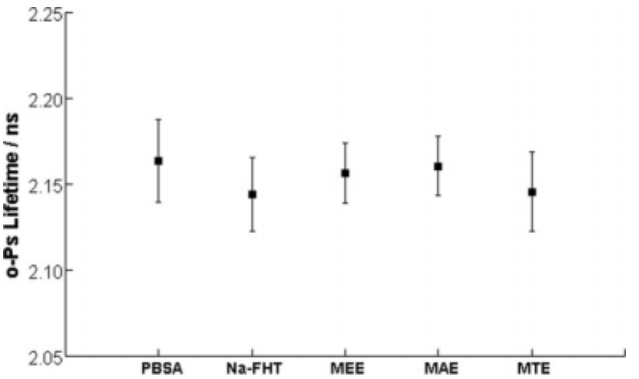

Figure 10 *o*-Ps lifetime obtained from host polymer and nanocomposites all with 5 wt % clay.

Figure 11 illustrates the *o*-Ps intensity measured from the polymer host, the unmodified clay nanocomposite and the modified clay nanocomposites. As can be seen, similar to *o*-Ps lifetime measurements, there is little difference in *o*-Ps intensity, which is indicative of pore concentration. Looking closely at the results, it seems that the modified clay nanocomposites may show slightly higher *o*-Ps intensities compared with the host matrix and the unmodified clay nanocomposite; however, this trend is within the error of the measurement (0.3%). *o*-Ps intensity does not seem to correlate with crystallinity as measured by DSC. DSC showed a small decrease in crystallinity for all of the nanocomposites, with Na–FHT–MAE having the lowest percentage crystallinity. Generally, a decrease in polymer crystallinity

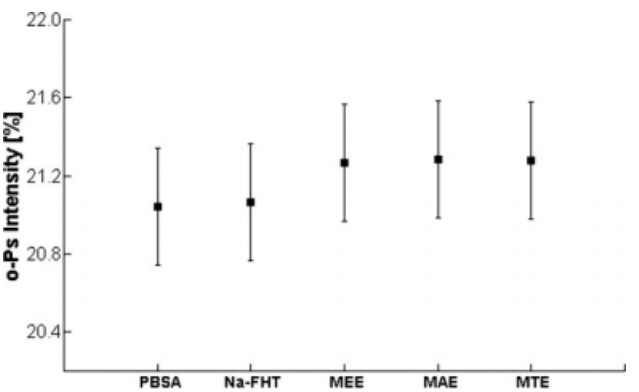

Figure 11 *o*-Ps Intensity obtained from host polymer and nanocomposites all with 5 wt % clay.

TABLE III
Thermal Behavior of Neat PBSA and 5 Wt % nanocomposites from DSC

Sample	Glass transition temperature (T_g °C)	Melting point (T_m °C)	Melting enthalpy of polymer (ΔH_m J/g)
Neat PBSA	−45.9°C	Peak 1: 85.7 Peak 2: 94.5	Peak 1: 8.7 Peak 2: 32.0 Total: 41.5
PBSA/Na–FHT	−43.8	Peak 1: 83.6 Peak 2: 93.9	Peak 1: 6.2 Peak 2: 33.6 Total: 39.8
PBSA/Na–FHT–MEE	−44.5	Peak 1: 80.4 Peak 2: 93.9	Peak 1: 2.6 Peak 2: 36.1 Total: 38.7
PBSA/Na–FHT–MAE	−43.3	Peak 1: 83.5 Peak 2: 95.4	Peak 1: 6.9 Peak 2: 30.0 Total: 36.9
PBSA/Na–FHT–MTE	−43.1	Peak 1: 82.0 Peak 2: 94.3	Peak 1: 5.5 Peak 2: 34.6 Total: 40.1

TABLE IV
Oxygen Permeability of Neat PBSA and Nanocomposites

Sample	Film thickness (μm)	O_2 permeability (cc/[m^2 day])	Permeation rate (cc-mm/[m^2 day])
Neat PBSA	265.0	155.8 ± 5.7	41.3 ± 0.4
PBSA:5 wt % Na–FHT	280.0	96.0 ± 0.2	26.8% ± 0.1 35% reduction
PBSA:5 wt % Na–FHT– MEE	277.5	70.6 ± 1.4	19.6% ± 0.2 53% reduction
PBSA:5 wt % Na–FHT–MAE	280.0	86.2 ± 0.2	24.1% ± 0.1 42% reduction
PBSA:5 wt % Na–FHT–MTE	280.0	94.7 ± 3.9	26.5% ± 0.4 36% reduction

results in an increase in *o*-Ps intensity, as *o*-Ps prefers to annihilate in the amorphous region of the polymer. The results presented do not agree with previous literature reports where the addition of filler into the polymer matrix resulted in a decrease in *o*-Ps intensity attributed to volume filling by nonporous filler particles.[21-23] PALS experiments were performed on the neat modified FHTs and an average *o*-Ps intensity of 20.3% was measured. Therefore, the absence of volume filling in the *o*-Ps intensity, is most likely owing to the filler having a similar *o*-Ps intensity as the neat polymer.

Permeability

The oxygen permeability of the neat PBSA was reduced by 35% purely by the addition of unmodified Na–FHT (see Table IV). TEM has shown that the unmodified Na–FHT was poorly dispersed, despite this the Na–FHT must have introduced some degree of tortuous path for the gas molecules. The addition of the modified Na–FHTs as finely dispersed Na–FHT–MEE and Na–FHT–MAE led to a higher reduction in oxygen permeability (53% and 42%, respectively) (see Table IV). TEM for these two systems has shown the platelet dispersion and orientation, resulting in a reduced gas permeability. The improved barrier properties are attributed to improved dispersion owing to better compatibility of these modified clays with the PBSA matrix. The DSC and PALS results confirm that the reduction in oxygen permeability was not because of increased levels of crystallinity or free volume changes, respectively.

CONCLUSIONS

Biodegradable aliphatic polyester–clay nanocomposites have been prepared by dispersing a series of organically modified synthetic FHTs into PBSA via high shear melt extrusion. Superior dispersions of nanoclays were confirmed using TEM (TEM)—showing highly oriented exfoliated structures. A reduction in oxygen permeability by 53% was observed in the well-dispersed flurohectorites modified with di poly(oxyethylene) alkyl methyl ammonium and dimethyl dialkyl ammonium. Nanoclay dispersion was found to depend on both chemical functionality and high initial d_{001} spacing (presence of longer alkyl chain hexadecyl and octodecyl groups in Na–FHT–MAE). It was concluded that this reduction in permeability was predominantly because of the tortuous path of oriented platelets and not from any change in crystallinity or amorphous phase free volume. The clay dispersion and orientation also led to significant increases in the mechanical properties (120% increase in modulus, 30% increase in notched impact strength).

The authors acknowledge Liz Goodall for XRD measurements.

References

1. Park, H.-M.; Lee, W.-K.; Park, C.-Y.; Cho, W.-J.; Ha, C.-S. J Mater Sci 2003, 38, 909.
2. Dean, K.; Yu, L.; Wu, D.-Y. Compos Sci Technol 2007, 67, 413.
3. Tunc, S.; Angellier, H.; Cahyana, Y.; Chalier, P.; Gontard, N.; Gastaldi, E. J Membr Sci 2007, 289, 159.
4. Zhang, X.; Do, M.; Dean, K.; Hoobin, P.; Burgar, I. Biomacromol 2007, 8, 345.

5. Di, Y.; Iannace, S.; Di Maio, E.; Nicolais, L. J Polym Sci Part B: Polym Phys 2003, 41, 670.
6. Di Maio, E.; Iannace, S.; Sorrentino, L.; Nicolais, L. Polymer 2004, 45, 8893.
7. Petersson, L.; Oksman, K.; Mathew, A. P. J Appl Polym Sci 2006, 102, 1852.
8. Ray, S. S.; Yamada, K.; Okamoto, M.; Fujimoto, Y.; Ogami, A.; Ueda, K. Polymer 2003, 44, 6633.
9. Paul, M. A.; Alexandre, M.; Degée, P.; Henrist, C.; Rulmont, A.; Dubois, P. Polymer 2003, 44, 443.
10. Thellen, C.; Orroth, C.; Froio, D.; Ziegler, D.; Lucciarini, J.; Farrell, R.; D'Souza, N.; Ratto, J. Polymer 2005, 46, 11716.
11. Lee, S. R.; Park, H. M.; Lim, H.; Kang, T.; Li, X.; Cho, W. J.; Ha, C. S. Polymer 2002, 43, 2495.
12. Lim, S. T.; Hyun, Y. H.; Choi, H. J.; Jhon, M. Chem Mater 2002, 14, 1839.
13. Ray, S. S.; Bousmina, M. Polymer 2005, 46, 12430.
14. Ray, S. S.; Bousmina, M.; Okamoto, K. Macromol Mater Eng 2005, 290, 759.
15. Someya, Y.; Nakazoto, T.; Teramoto, N.; Shibata, M. J Appl Polym Sci 2004, 91, 1463.
16. Shih, Y. F.; Wang, T. Y.; Jeng, R. J.; Wu, J. Y.; Teng, C. C. J Polym Environ 2007, 15, 151.
17. Ray, S. S.; Bousmina, M. Macromol Chem Phys 2006, 207, 1207.
18. Ray, S. S.; Bousmina, M. Polym Degrad Stab 2007, 92, 802.
19. Chang, J.; An, Y.; Sur, G. J Polym Sci Part B: Polym Phys 2003, 41, 94.
20. Di, Y.; Iannac, S.; Sanguigno, L.; Nicolais, L. Macromol Symp 2005, 228, 115.
21. Winberg, P.; Eldrup, M.; Pedersen, N. J.; van Es, M. A.; Maurer, F. H. J. Polymer 2005, 46, 8239.
22. Wang, S. J.; Liu, L. M.; Fang, P. F.; Chen, Z.; Wang, H. M.; Zhang, S. P. Radiat Phys Chem 2007, 76, 106.
23. Wang, B.; Qi, N.; Gong, W.; Li, X. W.; Zhen, Y. P. Radiat Phys Chem 2007, 76, 146.
24. Fujimaki, T. Polym Degrad Stab 1998, 59, 209.
25. Kansy, J. Nucl Instrum Methods Phys Res Sect A 1996, 374, 235.
26. Tao, S. J. J Chem Phys 1972, 56, 5499.
27. Eldrup, M.; Lightbody, D.; Sherwood, J. N. Chem Phys 1981, 63, 51.
28. Alonso, M.; Velasco, J. I.; Saja, J. A. Eur Polym J 1997, 33, 255.
29. Fornes, T. D.; Paul, D. R. Polymer 2003, 44, 3945.
30. Fornes, T. D.; Paul, D. R. Polymer 2003, 44, 4993.
31. John, J.; Mani, R.; Bhattacharya, M. J Polym Sci Part A: Polym Chem 2002, 40, 2003.
32. Ammala, A.; Lawrence, K. A.; Stark, R.; Webb, R. I.; Hill, A. J. J Mater Chem 2008, 18, 911.